Journal of Biomedical Optics

BiomedicalOptics.SPIEDigitalLibrary.org

Spectroscopic separation of Čerenkov radiation in high-resolution radiation fiber dosimeters

Arash Darafsheh
Rongxiao Zhang
Stephen Chad Kanick
Brian W. Pogue
Jarod C. Finlay

SPIE.

Spectroscopic separation of Čerenkov radiation in high-resolution radiation fiber dosimeters

Arash Darafsheh,[a,*] Rongxiao Zhang,[b] Stephen Chad Kanick,[c] Brian W. Pogue,[b,c] and Jarod C. Finlay[a,*]
[a]University of Pennsylvania, Department of Radiation Oncology, 3400 Civic Center Boulevard, Philadelphia, Pennsylvania 19104, United States
[b]Dartmouth College, Department of Physics and Astronomy, Hanover, New Hampshire 03755, United States
[c]Dartmouth College, Thayer School of Engineering, Hanover, New Hampshire 03755, United States

Abstract. We have investigated Čerenkov radiation generated in phosphor-based optical fiber dosimeters irradiated with clinical electron beams. We fabricated two high-spatial resolution fiber-optic probes, with 200 and 400 μm core diameters, composed of terbium-based phosphor tips. A generalizable spectroscopic method was used to separate Čerenkov radiation from the transmitted signal by the fiber based on the assumption that the recorded signal is a linear superposition of two basis spectra: characteristic luminescence of the phosphor medium and Čerenkov radiation. We performed Monte Carlo simulations of the Čerenkov radiation generated in the fiber and found a strong dependence of the recorded Čerenkov radiation on the numerical aperture of the fiber at shallow phantom depths; however, beyond the depth of maximum dose that dependency is minimal. The simulation results agree with the experimental results for Čerenkov radiation generated in fibers. The spectroscopic technique used in this work can be used for development of high-spatial resolution fiber micro dosimeters and for optical characterization of various scintillating materials, such as phosphor nanoparticles, in ionizing radiation fields of high energy. [DOI: 10.1117/1.JBO.20.9.095001]

Keywords: fiber optic; Čerenkov radiation; spectroscopy; ionizing radiation; dosimetry.

Paper 150312PRR received May 12, 2015; accepted for publication Jul. 31, 2015; published online Sep. 3, 2015.

1 Introduction

Fiber-optic probes in conjunction with scintillating materials are promising candidates for radiation therapy dosimetry, such as in high-dose rate brachytherapy,[1,2] intensity-modulated radiation therapy,[3] superficial therapy,[4] and stereotactic radiosurgery.[5] Real-time measurements, small physical size of the probe, high-spatial resolution, and ability of performing *in vivo* intracavity measurements are the main advantages of such probes. The working principle of such a device relies on the generation of an optical signal proportional to the absorbed dose in the irradiated scintillating medium, which is collected and transmitted by the optical fiber to a detector, usually a photodiode or photomultiplier tube. The total optical signal recorded by the detector, however, has unwanted components in addition to the useful scintillation signal. These artifactual signals, collectively termed "stem effect,"[6,7] are composed primarily of the Čerenkov radiation generated in the irradiated portion of the fiber together with a small contribution of the intrinsic fiber fluorescence in the case of plastic fibers. Only the scintillation emission from the scintillator is directly proportional to the amount of energy deposited in the scintillator, i.e., absorbed dose; therefore, the total signal must be corrected for the contribution of Čerenkov radiation in order to accurately measure the absorbed dose in the scintillator. Generation of Čerenkov radiation in the fiber, particularly at angles where it is dominant, imposes a limit on the physical dimensions and spatial resolution of plastic fiber scintillators in order to achieve a reliable signal-to-background ratio.

*Address all correspondence to: Arash Darafsheh, E-mail: arash.darafsheh@gmail.com; Jarod C. Finlay, E-mail: jarod.finlay@uphs.upenn.edu

Čerenkov radiation[8–11] occurs when charged particles traverse a dielectric medium with velocities greater than the phase velocity of light in that medium. It is a polarized, coherent, and directional emission; its direction is along the surface of a cone that makes the half-angle $\theta = \cos^{-1}(n\beta)^{-1}$ with the particle's track, where n is the refractive index of the medium and $\beta = v/c$ is the ratio of the velocity of the particle to that of light. Since the particle must travel faster than light, i.e., $v > c/n$, to induce Čerenkov radiation, its minimum energy is $E_{\min} = m_0c^2[(1-n^{-2})^{-1/2} - 1]$, where m_0 is the rest mass of the particle. For example, the threshold electron energies to generate Čerenkov radiation in water ($n = 1.33$) and pure silica ($n = 1.55$) are $E_{\min} = 264$ and 158 keV, respectively. The number of Čerenkov photons generated by a charged particle with z times the charge of an electron along path length l in the wavelength region between λ_1 and λ_2 ($\lambda_1 < \lambda_2$), is proportional to λ^{-2}, and is given by $N = 2\pi\alpha z l(\lambda_1^{-1} - \lambda_2^{-1})[1 - (n\beta)^{-2}]$, where $\alpha \approx 137^{-1}$ is the fine structure constant.[11] Čerenkov radiation has a continuous spectrum spanning from near ultraviolet to near infrared with light intensity decreasing proportional to λ^{-3} as the wavelength increases; the spectrum of Čerenkov radiation is restricted from both ends of the visible spectrum by the absorption spectrum of the material in which it is generated.

Čerenkov radiation has been the subject of considerable research in recent years for potential applications in life sciences and engineering. A number of articles have appeared introducing its potential applications in molecular imaging,[12–19] monitoring of tissue optical properties,[20] ionizing radiation beam monitoring, quality assurance and dosimetry,[21–33] and particle detection.[34–38] When optical fibers pass through ionizing

radiation fields of high energy, as in fiber-optic dosimetry, Čerenkov radiation generated inside the fibers' core is guided through the fiber if the emitted ray hits the core-cladding boundary with an angle greater than the critical angle satisfying the total internal reflection condition required for guided rays. Transmission of Čerenkov radiation is, therefore, dependent on the angle between the particle's track and the fiber's axis. Therefore, the recorded raw signal is not directly related to the dose absorbed by the scintillator. Čerenkov radiation signal is strongest when the angle between the fiber's axis and particle's track is close to the Čerenkov cone half-angle. It should be mentioned that depending on the dosimetry protocol, Čerenkov light generated in the optical fiber may be the useful signal. In scintillation fiber-optic dosimetry, however, Čerenkov light is an unwanted background signal and separating it from the total optical signal is crucial; using raw signals without removing it would lead to errors higher than 20%.

Four general methods have been applied to separate the Čerenkov light from the total optical signal: (1) Subtraction method,[6,39] where a parallel fiber identical to the one that is connected to the scintillating piece is used to generate similar background light that can be subtracted from the total signal. For fields with high-dose gradient, however, such a technique is not reliable. (2) Optical filtering,[40] where a long-wavelength-emitting scintillator in conjunction with a long-pass filter is used to selectively measure the signal in longer wavelengths of the spectrum where contribution of Čerenkov radiation is minimal due to its λ^{-3} profile. Nevertheless, this method is not very effective since the filtered signal is still contaminated with the Čerenkov radiation due to the fact that the Čerenkov radiation has a continuous spectrum. (3) Temporal separation[41] that relies on different time scales associated with Čerenkov radiation and the scintillation process. This method requires fast responding electronics and works only with pulsed radiation fields. (4) Chromatic removal,[42–44] which is the current state-of-the-art method and requires two different optical filters to measure the signal at two different spectral regions; the dose is then calculated by using coefficients obtained from calibration.

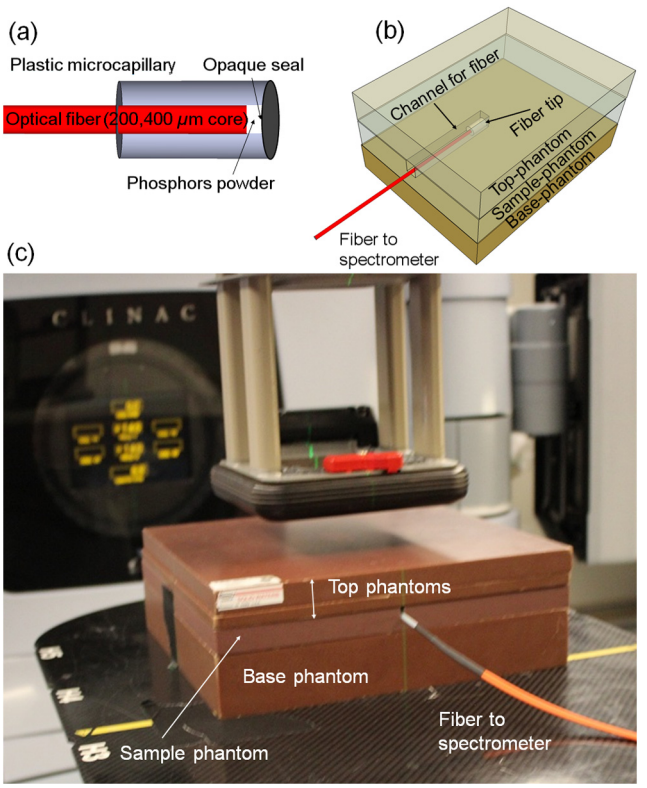

Fig. 1 Schematic illustration of: (a) fiber-optic probe design and (b) the experimental setup. (c) Experimental setup with a clinical linac: the fiber probe was positioned in a virtual water phantom labeled as the sample-phantom and additional phantom layers (labeled as top phantoms) were placed sequentially over the sample-phantom.

It should be noted that it has been suggested[45] that the use of hollow waveguides with an air core instead of conventional solid core fibers would reduce the deteriorating effect of Čerenkov radiation because the production of Čerenkov light is minimal in air since its refractive index is close to 1; such hollow waveguides, however, have optimal design parameters for transmission of infrared wavelengths,[46,47] whereas the scintillators of interest here emit primarily visible light.

In this work, we address two aspects of the problem of Čerenkov contamination in optical fibers used for scintillation dosimetry: first, we demonstrate the rigorous spectroscopic separation of the contributions from scintillator emission and Čerenkov radiation using a low-cost single-channel spectrometer and a straightforward linear superposition fitting algorithm. This allows detection of the scintillation signal using a single optical fiber and robust rejection of Čerenkov contamination. Second, using Monte Carlo simulation, we investigate in detail the dependence of the Čerenkov contamination on the details of the optical fiber used for detection, specifically on the numerical aperture. These results explain the variations in the degree of Čerenkov contamination with depth in electron beams, and inform the design of future generations of high-resolution optical fiber dosimetry systems.

2 Materials and Methods

In order to experimentally study the induced Čerenkov radiation in fiber dosimeters, we fabricated high-resolution fiber-optic microprobes and performed luminescence spectroscopy. Our dosimetry system consisted of four components: (1) a phosphor-based probe to convert the absorbed dose to an optical signal, (2) an optical fiber to transmit the generated light from the probe to the spectrometer, (3) a spectrometer to acquire the spectrum of light collected by the fiber, and (4) a computer for signal processing to calculate the luminescence of phosphors.

Figure 1(a) is a schematic illustration of the probe design. An ~1 to 3 mm layer of TbF_3 (Sigma-Aldrich) in the form of a white powder was packed in a plastic capillary (Cole-Parmer). The distal end of the capillary was optically sealed. A 15-m long silica optical fiber (FT400UMT, Thorlabs) with numerical aperture NA = 0.39 (pure silica core with refractive index 1.51 and fluoropolymer cladding with index 1.46 at $\lambda = 500$ nm) and core diameter of 400 μm was inserted 3 mm into the capillary from the other end to capture and transport the emitted light from the phosphors to the spectrometer. The size match between internal diameter of the plastic capillary and the external diameter of the fiber provided tight packing of the phosphors and the fiber. In another probe design, we used an optical fiber with a 200-μm core diameter (FT200UMT, Thorlabs) with NA = 0.39. The effective radiation-sensitive portion of our probes is ~0.1 to 0.5 mm^3.

Optical spectroscopy was performed using a thermoelectrically cooled CCD array spectrometer (BTC112E, BWTEK Inc.) with a 0.4-nm spectral resolution. In order to minimize direct interaction of the ionizing radiation with its CCD, the

spectrometer was placed outside the treatment room. Dark current spectra were obtained by collecting spectra with the spectrometer's input aperture covered, and were subtracted from each spectrum acquired. The spectra were corrected for wavelength-dependent instrument response and wavelength-dependent transmission of fibers using an instrument-specific calibration function. This function was determined for each fiber by taking the ratio of the measured spectrum of a lamp with an NIST-traceable calibration (LS1-cal, Ocean Optics) to its known spectrum.

In order to study Čerenkov radiation generated in the fiber and evaluate the performance of the fiber probes, we performed optical characterization experiments in a tissue equivalent environment by using virtual water phantoms (standard imaging). 15 cm of the distal end of the fiber was positioned in a drilled channel parallel to the sides and passing along the center of a $30 \times 30 \times 1$ cm^3 virtual water phantom, labeled "sample-phantom" in Fig. 1(b). The fiber was completely embedded in the sample-phantom, allowing us to place additional phantom layers on top of the sample-phantom. Additional phantom layers were sequentially added after each measurement to provide measurements at different phantom depths. In all cases, the source-to-surface-distance (SSD), measured to the top surface of the top most phantom, was adjusted to 100 cm. In all experiments, a 5-cm base layer of virtual water phantom was placed under the sample-phantom. A black rubberized fabric (BK5, Thorlabs) was used to cover the sample- and base-phantoms during the experiments to assure no background light, such as the alignment laser or device indicator light, is collected by the fiber.

The fiber probe was irradiated by a 6-MeV electron beam in a square 10×10 cm^2 field generated by using a clinical medical linear accelerator (Clinac 2100 IX, Varian Medical Systems), see Fig. 1(c). The selected beam energy is much greater than the energy threshold required for emission of Čerenkov radiation in pure silica ($E_{\min} \approx 0.158$ MeV). The dose rate in all experiments was set to 6 Gy/min at the depth of the maximum dose.

The recorded luminescence signal (S_{tot}) by the spectrograph was considered as the linear superposition of two basis components: luminescence from the phosphors (L_{ph}) and the Čerenkov radiation ($\check{C}_f$) generated in the fiber. Therefore, the recorded spectrum in each case, corrected for instrument response, was analyzed as a linear combination of basis luminescence spectra using a singular value decomposition (SVD) fitting algorithm implemented in MATLAB®, similar to that used previously[48] for fitting fluorescent spectra in studying the photobleaching kinetics of photosensitizers in photodynamic therapy. The basis spectrum for the Čerenkov radiation is calculated from the theoretical λ^{-3} dependency expected for Čerenkov radiation, where λ is the wavelength of light. We experimentally verified the λ^{-3} dependency by curve fitting to spectra, obtained from irradiated standalone fibers in various conditions. The basis spectrum for the characteristic luminescence of phosphors was obtained according to the following manner. First, we recorded the spectrum of the irradiated fiber probe with its phosphor tip connected. Then we removed the phosphor tip and recorded the spectrum of the irradiated bare fiber. By subtracting the latter from the former, we obtained the basis spectrum for the luminescence of the phosphors. We verified that basis spectrum by irradiating the phosphors with incident beams of energies below the threshold for generating Čerenkov radiation. The SVD fitting algorithm has additional Fourier terms to take into account the potential presence of any other contributions in the fiber. The two basis spectra and the Fourier series (F_0) are fit to the instrument-corrected data using Eq. (1),

$$S_{\text{tot}} = a_{100} L_{\text{ph}} + b_{100} \check{C}_f + c_{1.4} F_0, \quad (1)$$

where the numbers in subscript are the weights used in the SVD fitting algorithm. This choice of the weighting factors provided reliable fits to the experimental data. It should be noted that their exact values are not critical as the SVD fits were remarkably insensitive to the choice of weighting factors. The coefficients a_{100} and b_{100} in each beam condition were considered as the measure of the absorbed dose and Čerenkov radiation, respectively.[49–51]

Monte Carlo simulation was conducted by using the GEANT4-based toolkit GAMOS for Monte Carlo modeling to stochastically simulate radiation transport, dose deposition, and Čerenkov radiation emission. A phase space file (from the IAEA database) of a 10×10 cm^2 6-MeV electron beam for the LINAC (Varian Clinic 2100CD) was adopted as the irradiating source. The phase space file was used to irradiate the cubic phantom (water equivalent, $30 \times 30 \times 30$ cm^3) at SSD = 100 cm. Optical fibers were modeled and placed at depths from 1 to 49 mm with an increment of 2 mm. For any Čerenkov photon generated in the fiber, initial positions, directions, and energies were recorded. Any Čerenkov photon with initial directions that fell into the collection angle of the fiber was assumed to be detectable. Additionally, radiation doses deposited in each fiber were scored. In total, 10^9 primary particles were initialized from the phase space file.

3 Results and Discussion

The normalized basis spectra for the Čerenkov radiation with λ^{-3} wavelength dependency and the luminescence of the TbF_3 phosphors with peaks at $\lambda = 489$, 542, 587, and 620 nm are presented in Figs. 2(a) and 2(b), respectively.

We performed measurements at various exposure times in the range from 0.5 to 20 s and dose rates from 1 to 200 cGy/min and found that ~2 cGy is the minimum dose that can be measured with less than 4% uncertainty. We selected 20 s exposure times for the rest of the measurements.

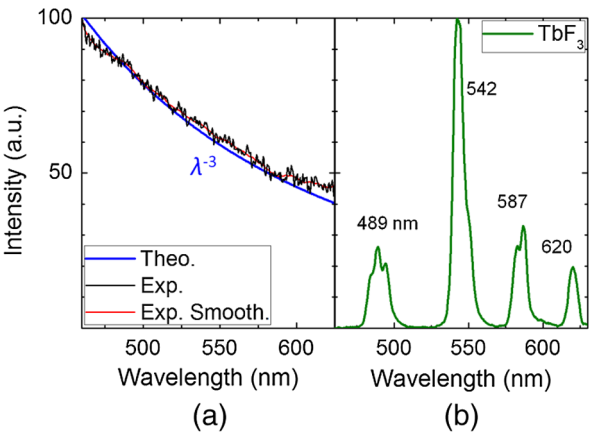

Fig. 2 Basis spectra corresponding to (a) Čerenkov radiation and (b) luminescence of TbF_3 phosphors (peaks are at $\lambda = 489$, 542, 587, and 620 nm) used for singular value decomposition method. Both spectra were normalized to have maximum value of 100 within the spectral range of $\lambda = 460$ to 630 nm.

A typical recorded spectrum at a 1.5-cm phantom depth and the SVD results from the irradiated fiber probe are presented in Fig. 3. The measured spectrum is a superposition of the cathodoluminescence signal from TbF_3 with four characteristic peaks at $\lambda = 489$, 542, 587, and 620 nm due to the f-f transition of a terbium ion, on a continuous Čerenkov radiation background, with λ^{-3} wavelength dependence. By using the SVD algorithm, we decomposed the recorded signal into its constituent components. Figure 3(b) shows the decomposed spectra, i.e., emission of TbF_3 and Čerenkov radiation, corresponding to the spectrum presented in Fig. 3(a). The presence of four characteristic features in the terbium spectrum makes the spectral separation of Čerenkov radiation generated in the fiber more robust to noise. We observed an excellent agreement between the recorded spectrum and the fit obtained from the linear combination of the decomposed spectra, as illustrated in Fig. 3(b), demonstrating the feasibility of the spectral separation of Čerenkov radiation.

Figure 4(a) shows the simulation results of the absorbed dose, total Čerenkov radiation generated in the fiber, and the amount of Čerenkov radiation coupled to the fiber, as a function of depth in the phantom for a 6-MeV monoenergetic electron beam. All values were normalized to 100% at a 1.5-cm depth. The dose exhibits the well-known characteristics of a 6-MeV electron beam in water, with a depth of maximum dose (d_{max}) around 1.5 cm resulting from the interplay of electron scattering and collisional energy loss.[52] Monte Carlo simulation results reveal a considerable discrepancy between the total generated Čerenkov radiation and the Čerenkov radiation coupled to the fiber. The discrepancy arises mainly from the fact that not all of the generated Čerenkov photons lie within the acceptance cone of the fiber, as schematically illustrated in Fig. 5. However, at depths beyond the depth of the maximum dose, the normalized total and coupled Čerenkov radiation curves converge and follow the same trend as the absorbed dose. When the effect of the NA of the fiber is taken into account in the simulation, there

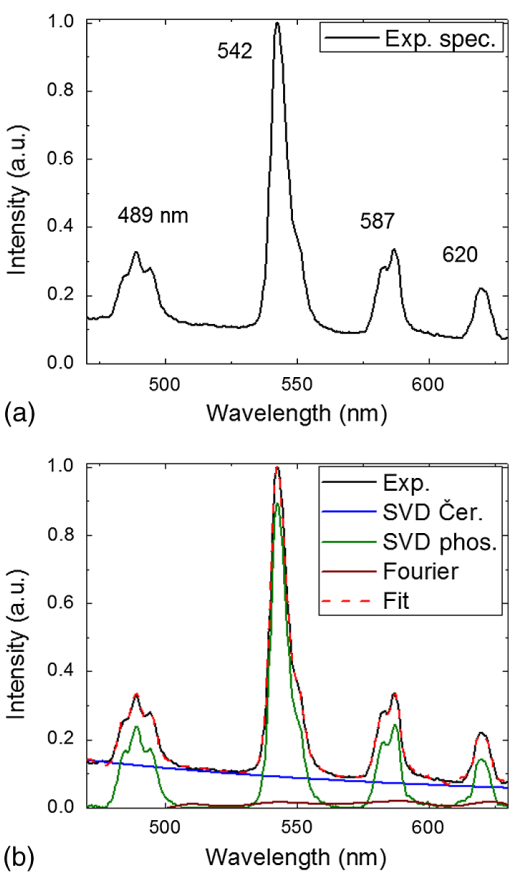

Fig. 3 (a) Recorded spectrum from the Tb-based probe showing cathodoluminescence of TbF_3 with peaks at $\lambda = 489$, 542, 587, and 620 nm superimposed on a continuous Čerenkov radiation background. The probe was irradiated at 1.5-cm phantom depth by a 6 MeV electron beam. (b) The resultant decomposed spectra of luminescence of terbium and Čerenkov radiation generated in the fiber. There is an excellent agreement between the measured spectrum and linear superposition of the decomposed spectra.

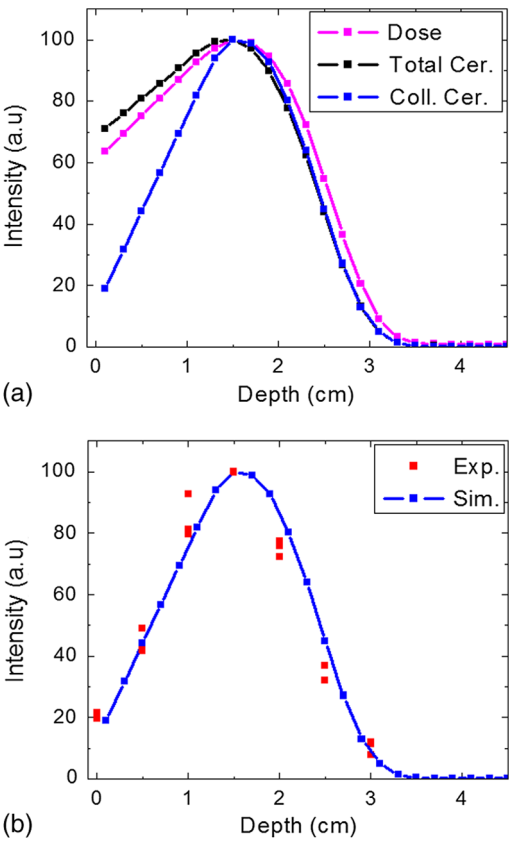

Fig. 4 (a) Monte Carlo simulation results of absorbed dose, total Čerenkov radiation generated in the fiber, and coupled Čerenkov radiation to the fiber (NA = 0.39) as a function of phantom depth for a monoenergetic 6-MeV electron beam with 10×10 cm^2 field size. (b) Comparison with the experimental results and Monte Carlo simulation.

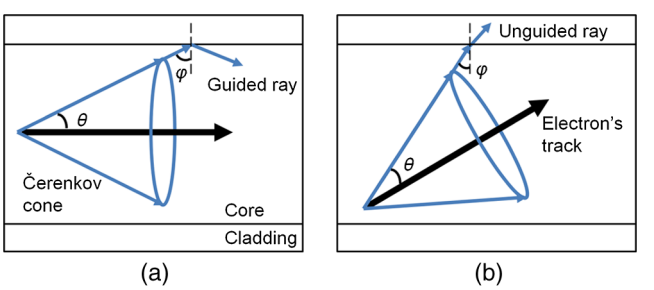

Fig. 5 Schematic illustration of Čerenkov radiation generated in the fiber when it is (a) guided through and (b) leaked from the fiber. θ is the Čerenkov semicone angle and φ is the critical angle.

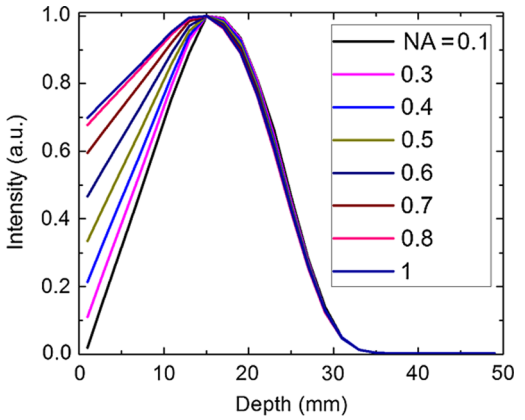

Fig. 6 Monte Carlo simulation results of the transmitted Čerenkov radiation by the fiber, irradiated with 6-MeV electron beam, as a function depth for different values of fiber numerical aperture in the range NA = 0.1 to 1.

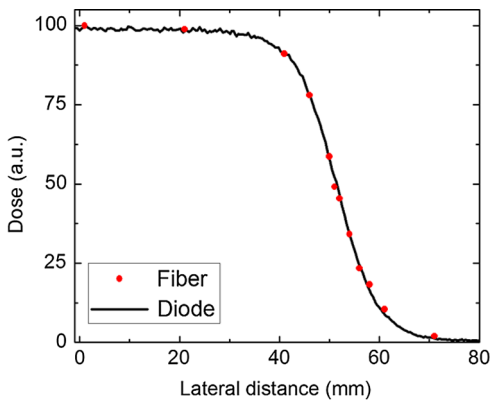

Fig. 7 Spatial beam profile at the phantom depth of maximum dose (d_{max} = 1.5 cm) for 6-MeV electron beam measured by the fiber probe compared to electron diode measurements.

is a good agreement between the calculated fit based on the SVD and the experimental data (coefficients b_{100}), as illustrated in Fig. 4(b).

The effect of the numerical aperture of the fiber on the Čerenkov radiation collected by the fiber was studied through Monte Carlo simulation. The NA of the fiber was changed from 0.1 to 1. The resulting ratios of the collected Čerenkov radiation to its maximum at d_{max} are shown in Fig. 6. We found that the intensity of the collected Čerenkov radiation in shallow phantom depths, i.e., in the build-up region, strongly depends on the NA of the fiber. This is due to the fact that the intensity of Čerenkov radiation strongly depends on the angle between the fiber axis and the electron trajectory, and the electrons at shallow depths are oriented primarily in the beam direction, perpendicular to the fiber axis. However, beyond the depth d_{max}, the dependency on the NA is minimal due to the angular spread of the electron beam, see Fig. 6.

The dose dependency of the luminescence of the Tb-based probes was studied by electron beam spatial profile measurement at the 1.5-cm phantom depth. The 200-μm core fiber probe was used in this study. The field size at 100-cm SSD was 10×10 cm^2 and the table was laterally moved to perform measurements at each point to collect data from 12 points from the center of the beam to a 7-cm lateral distance. The a_{100} coefficients obtained from the SVD fits, normalized to that corresponding to the maximum dose at the center of the beam, were used to measure the beam profile. For comparison, the profile measured by a diode-based radiation detector designed for measurements in electron beams is shown in the same figure. This profile was acquired as part of the commissioning procedure for the linear accelerator, in accordance with standard[53] commissioning procedures. In Fig. 7, the measured spatial beam profile is presented in comparison to the measurements performed by the electron diode that shows an excellent agreement (less than 1% deviation) between the two measurements.

4 Conclusions

We have investigated Čerenkov radiation generated in irradiated optical fibers and found that at depths shallower than the depth of maximum dose (build-up region), the intensity of the Čerenkov radiation coupled through the fiber is highly dependent on the numerical aperture of the fiber. However, beyond the depth of maximum dose, this effect disappears due to the angular spread of the electron beam. We used a generalizable method for separation of Čerenkov radiation generated in irradiated optical fibers based on optical spectroscopy measurements. This method works in fiber-optic applications, where optical fibers pass through high-energy ionizing radiation fields. We showed that the fiber-optic dosimetry of ionizing radiation fields based on phosphor-tipped fibers is feasible with submillimeter resolution provided that spectral separation of Čerenkov radiation is rigorously performed. The experimental method and apparatus developed in this work provide a robust platform for designing fiber-optic micro dosimeters and optical characterization of nanophosphors irradiated by medical beams to investigate them as potential imaging or therapeutic agents, e.g., when they are conjugated with photosensitizers used in photodynamic therapy.[54–56]

Acknowledgments

This work was supported by the Department of Radiation Oncology at the University of Pennsylvania and the American Cancer Society (IRG-78-002-28).

References

1. J. Lambert et al., "A plastic scintillation dosimeter for high dose rate brachytherapy," *Phys. Med. Biol.* **51**(21), 5505–5516 (2006).
2. F. Therriault-Proulx et al., "A phantom study of an *in vivo* dosimetry system using plastic scintillation detectors for real-time verification of 192Ir HDR brachytherapy," *Med. Phys.* **38**(5), 2542–2551 (2011).
3. M. Guillot et al., "A new water-equivalent 2D plastic scintillation detectors array for the dosimetry of megavoltage energy photon beams in radiation therapy," *Med. Phys.* **38**(12), 6763–6774 (2011).
4. F. Lessard et al., "Validating plastic scintillation detectors for photon dosimetry in the radiologic energy range," *Med. Phys.* **39**(9), 5308–5316 (2012).
5. J. C. Gagnon et al., "Dosimetric performance and array assessment of plastic scintillation detectors for stereotactic radiosurgery quality assurance," *Med. Phys.* **39**(1), 429–436 (2012).
6. S. Beddar, T. R. Mackie, and F. H. Attix, "Cerenkov light generated in optical fibres and other light pipes," *Phys. Med. Biol.* **37**(4), 925–935 (1992).
7. F. Therriault-Proulx et al., "On the nature of the light produced within PMMA optical light guides in scintillation fiber-optic dosimetry," *Phys. Med. Biol.* **58**(7), 2073–2084 (2013).
8. P. A. Čerenkov, "Visible emission of clean liquids by action of gamma radiation," *Dokl. Akad. Nauk SSSR* **2**, 451–454 (1934).

9. P. Čerenkov, "Visible radiation produced by electrons moving in a medium with velocities exceeding that of light," *Phys. Rev.* **52**(4), 378–379 (1937).
10. I. Frank and I. Tamm, "Coherent visible radiation of fast electrons passing through matter," *C. R. (Dokl.) Acad. Sci. URSS* **14**(3), 109–114 (1937).
11. J. V. Jelly, *Čerenkov Radiation and Its Applications*, Pergamon Press, London (1958).
12. R. S. Dothager et al., "Cerenkov radiation energy transfer (CRET) imaging: a novel method for optical imaging of PET isotopes in biological systems," *PLoS One* **5**(10), e13300 (2010).
13. M. A. Lewis et al., "On the potential for molecular imaging with Cerenkov luminescence," *Opt. Lett.* **35**(23), 3889–3891 (2010).
14. A. Ruggiero et al., "Cerenkov luminescence imaging of medical isotopes," *J. Nucl. Med.* **51**(7), 1123–1130 (2010).
15. G. Lucignani, "Cerenkov radioactive optical imaging: a promising new strategy," *Eur. J. Nucl. Med. Mol. Imaging.* **38**(3), 592–595 (2011).
16. Y. Xu, H. Liu, and Z. Cheng, "Harnessing the power of radionuclides for optical imaging: Cerenkov luminescence imaging," *J. Nucl. Med.* **52**(12), 2009–2018 (2011).
17. D. L. Thorek et al., "Quantitative imaging of disease signatures through radioactive decay signal conversion," *Nat. Med.* **19**(10), 1345–1350 (2013).
18. R. Zhang et al., "Cherenkov-excited luminescence scanned imaging," *Opt. Lett.* **40**(5), 827–830 (2015).
19. R. Zhang et al., "Cerenkov radiation emission and excited luminescence (CREL) sensitivity during external beam radiation therapy: Monte Carlo and tissue oxygenation phantom studies," *Biomed. Opt. Express* **3**(10), 2381–2394 (2012).
20. R. Zhang et al., "Oxygen tomography by Čerenkov-excited phosphorescence during external beam irradiation," *J. Biomed. Opt.* **18**(5), 050503 (2013).
21. J. L. Demers et al., "Čerenkov excited fluorescence tomography using external beam radiation," *Opt. Lett.* **38**(8), 1364–1366 (2013).
22. A. K. Glaser et al., "Projection imaging of photon beams by the Čerenkov effect," *Med. Phys.* **40**(1), 012101 (2013).
23. A. K. Glaser et al., "Projection imaging of photon beams using Čerenkov-excited fluorescence," *Phys. Med. Biol.* **58**(3), 601–619 (2013).
24. A. K. Glaser et al., "Three-dimensional Čerenkov tomography of energy deposition from ionizing radiation beams," *Opt. Lett.* **38**(5), 634–636 (2013).
25. K. W. Jang et al., "Application of Cerenkov radiation generated in plastic optical fibers for therapeutic photon beam dosimetry," *J. Biomed. Opt.* **18**(2), 027001 (2013).
26. R. Zhang et al., "Superficial dosimetry imaging based on Cerenkov emission for external beam radiotherapy with megavoltage x-ray beam," *Med. Phys.* **40**(10), 101914 (2013).
27. R. Zhang et al., "Superficial dosimetry imaging of Cerenkov emission in electron beam radiotherapy of phantoms," *Phys. Med. Biol.* **58**(16), 5477–5493 (2013).
28. R. Zhang et al., "Real-time in vivo Cherenkoscopy imaging during external beam radiation therapy," *J. Biomed. Opt.* **18**(11), 110504 (2013).
29. A. K. Glaser et al., "Video-rate optical dosimetry and dynamic visualization of IMRT and VMAT treatment plans in water using Cherenkov radiation," *Med. Phys.* **41**(6), 062102 (2014).
30. A. K. Glaser et al., "Optical dosimetry of radiotherapy beams using Cherenkov radiation: the relationship between light emission and dose," *Phys. Med. Biol.* **59**(14), 3789–3811 (2014).
31. Y. Helo et al., "Imaging Cerenkov emission as a quality assurance tool in electron radiotherapy," *Phys. Med. Biol.* **59**(8), 1963 (2014).
32. L. A. Jarvis et al., "Cherenkov video imaging allows for the first visualization of radiation therapy in real time," *Int. J. Radiat. Oncol. Biol. Phys.* **89**(3), 615–622 (2014).
33. R. Zhang et al., "Cherenkoscopy based patient positioning validation and movement tracking during post-lumpectomy whole breast radiation therapy," *Phys. Med. Biol.* **60**(1), L1–L14 (2015).
34. B. Brichard et al., "Fibre-optic gamma-flux monitoring in a fission reactor by means of Cerenkov radiation," *Meas. Sci. Technol.* **18**(10), 3257–3262 (2007).
35. J. S. Cho et al., "Cerenkov radiation imaging as a method for quantitative measurements of beta particles in a microfluidic chip," *Phys. Med. Biol.* **54**(22), 6757–6771 (2009).
36. Z. W. Bell et al., "Measurement of neutron yields from UF4," *IEEE Trans. Nucl. Sci.* **57**(4), 2239–2246 (2010).
37. K. W. Jang et al., "Feasibility of fiber-optic radiation sensor using Cerenkov effect for detecting thermal neutrons," *Opt. Express* **21**(12), 14573–14582 (2013).
38. W. J. Yoo et al., "Development of a Cerenkov radiation sensor to detect low-energy beta-particles," *Appl. Radiat. Isot.* **81**, 196–200 (2013).
39. W. J. Yoo et al., "Development of a fiber-optic dosimeter based on modified direct measurement for real-time dosimetry during radiation diagnosis," *Meas. Sci. Technol.* **24**(9), 094022 (2013).
40. S. F. de Boer, A. S. Beddar, and J. A. Rawlinson, "Optical filtering and spectral measurements of radiation-induced light in plastic scintillation dosimetry," *Phys. Med. Biol.* **38**, 945–958 (1993).
41. M. A. Clift, P. N. Johnston, and D. V. Webb, "A temporal method of avoiding the Cerenkov radiation generated in organic scintillator dosimeters by pulsed mega-voltage electron and photon beams," *Phys. Med. Biol.* **47**, 1421–1433 (2002).
42. J. M. Fontbonne et al., "Scintillating fiber dosimeter for radiation therapy accelerator," *IEEE Trans. Nucl. Sci.* **49**(5), 2223–2227 (2002).
43. A. M. Frelin et al., "Spectral discrimination of Čerenkov radiation in scintillating dosimeters," *Med. Phys.* **32**(9), 3000–3006 (2005).
44. M. Guillot et al., "Spectral method for the correction of the Cerenkov light effect in plastic scintillation detectors: a comparison study of calibration procedures and validation in Cerenkov light-dominated situations," *Med. Phys.* **38**(4), 2140–2150 (2011).
45. J. Lambert et al., "Cerenkov-free scintillation dosimetry in external beam radiotherapy with an air core light guide," *Phys. Med. Biol.* **53**(11), 3071–3080 (2008).
46. J. A. Harrington, "A review of IR transmitting, hollow waveguides," *Fiber Integr. Opt.* **19**(3), 211–227 (2000).
47. A. Darafsheh, "Optical super-resolution and periodical focusing effects by dielectric microspheres," PhD Dissertation, University of North Carolina at Charlotte (2013).
48. J. C. Finlay et al., "Porphyrin bleaching and PDT-induced spectral changes are irradiance dependent in ALA-sensitized normal rat skin in vivo," *Photochem. Photobiol.* **73**(1), 54–63 (2001).
49. A. Darafsheh et al., "Separation of Čerenkov radiation in irradiated optical fibers by optical spectroscopy," *Proc. SPIE* **9315**, 93150Q (2015).
50. A. Darafsheh et al., "Phosphor-based fiber optic microprobes for ionizing beam radiation dosimetry," *Proc. SPIE* **9317**, 93170R (2015).
51. A. Darafsheh et al., "Phosphor-based fiber optic probes for proton beam characterization," *Med. Phys.* **42**(6), 3476 (2015).
52. F. M. Khan, *The Physics of Radiation Therapy*, 3rd ed., Lippincott Williams & Wilkins, Philadelphia (2009).
53. B. J. Gerbi et al., "Recommendations for clinical electron beam dosimetry: supplement to the recommendations of task group 25," *Med. Phys.* **36**(7), 3239–3279 (2009).
54. A. Darafsheh et al., "Characterization of rare-earth-doped nanophosphors for photodynamic therapy excited by clinical ionizing radiation beams," *Proc. SPIE* **9308**, 930812 (2015).
55. A. Darafsheh et al., "Optical characterization of novel terbium-doped nanophosphors excited by clinical electron and photon beams for potential use in molecular imaging or photodynamic therapy," *Med. Phys.* **41**, 436 (2014).
56. J. C. Finlay and A. Darafsheh, "Light sources, drugs, and dosimetry," in *Biomedical Optics in Otorhinolaryngology, Head and Neck Surgery: Principles and Practices*, B. Wong and J. Ilgner, Eds., Springer, New York (2015).

Arash Darafsheh is a medical physics resident at the University of Pennsylvania. He holds a BSc in electrical engineering, an MSc in radiation medicine engineering, an MSc and PhD in optical science and engineering, and a postgraduate certificate in medical physics. His research interests are in the areas of optics and photonics and medical physics. He has pioneered the immersed microsphere-assisted super-resolution imaging technique. He has published over 50 papers, a book chapter, and a patent.

Rongxiao Zhang received his BS degree in physics from the University of Science and Technology of China and his PhD in medical physics from Dartmouth College, Hanover, New Hampshire, in 2010 and 2015, respectively. Currently, he is a medical physics

resident in the Harvard Medical Physics program. His research focuses on biomedical applications of Čerenkov emission in radiation therapy, especially for the purposes of dosimetry and biomedical sensing.

Stephen Chad Kanick is an assistant professor in the Thayer School of Engineering at Dartmouth College. He obtained a PhD in chemical engineering from the University of Pittsburgh and completed a postdoctoral appointment at the Erasmus Medical Center in Rotterdam, the Netherlands. His research focuses on the development of new quantitative spectroscopy approaches that are useful for diagnosing pathologies, guiding surgeries, and monitoring administered therapies. He recently received a Career Development Award from the NIH/NCI.

Brian W. Pogue is professor of engineering, physics and astronomy, and surgery at Dartmouth College in Hanover, New Hampshire. He received his PhD in medical/nuclear physics from McMaster University, Canada. He works in the area of optics in medicine, with a focus on novel imaging systems for characterizing cancer and imaging therapy. He has published over 230 peer-reviewed papers in the areas of biomedical optics, and his research is funded by the National Cancer Institute.

Jarod C. Finlay is an assistant professor in the Department of Radiation Oncology at the University of Pennsylvania. He completed his PhD at the University of Rochester and postdoctoral study at the University of Pennsylvania in the areas of tissue optics and photodynamic therapy dosimetry. His work focuses on preclinical and clinical photodynamic therapy, and optical imaging for dosimetry in photodynamic and ionizing radiation therapies. He has published over 25 peer-reviewed papers and holds two patents.